

Controlling thermodynamics of a quantum heat engine with modulated amplitude drivings

Sajal Kumar Giri¹ and Himangshu Prabal Goswami^{2, a)}

¹⁾*Department of Chemistry, Northwestern University, 2145 Sheridan Rd., Evanston, IL 60208, United States*

²⁾*Department of Chemistry, Gauhati University, Jalukbari, Guwahati-781014, Assam, India*

(Dated: 30 March 2022)

External driving of bath temperatures with a phase difference of a nonequilibrium quantum engine leads to the emergence of geometric effects on the thermodynamics. In this work, we modulate the amplitude of the external driving protocols by introducing envelope functions and study the role of geometric effects on the flux, noise and efficiency of a four-level driven quantum heat engine coupled with two thermal baths and a unimodal cavity. We observe that having a finite width of the modulation envelope introduces an additional control knob for studying the thermodynamics in the adiabatic limit. The optimization of the flux as well as the noise with respect to thermally induced quantum coherences becomes possible in presence of geometric effects, which is hitherto not possible with sinusoidal driving without an envelope. We also report the deviation of the slope and generation of an intercept in the standard expression for efficiency at maximum power as a function of Carnot efficiency in presence of geometric effects under the amplitude modulation. Further, a recently developed universal bound on the efficiency obtained from thermodynamic uncertainty relation is shown not to hold when a small width of the modulation envelope along with a large value of cavity temperature is maintained.

I. INTRODUCTION

Quantum heat engines (QHEs) have come a long way from the theoretically predicted Schulz-duBois engine¹ to experimentally realizable engines. Notable examples include Rb based cold atomic setup², Li-based Fermi gas³, diamond based N-vacancy centres⁴, Paul-trapped Yb and Ca ion setups^{5,6} and utilizing proton's nuclear spin dissolved in 13-C labeled CHCl_3 ⁷. Role of coherences on the quantum thermodynamic and transport properties, establishing the validity of nonequilibrium fluctuation theorems, thermodynamic uncertainty relationships (TUR) are now being investigated experimentally and compared with the results obtained from several theoretically established models⁸⁻¹¹. Most of the theories are based on Markovian master equations and have seemed to agree pretty well with experimental observations^{10,12}. Success of such master equations in understanding several steady-state properties of QHEs led to the widespread use of another class of master equations that theoretically predict dynamics of quantum systems where system parameters are modulated in time, usually called driven dynamics¹³⁻¹⁵. Toy models based on QHEs are often a common choice to study driven dynamics using adiabatic master equations^{13,16}. In such driven systems, periodic or nonperiodic modulation of a system parameter (like energy, reservoir temperature etc.) in an adiabatic fashion¹⁷⁻²¹ has led to the theoretical prediction of exotic properties such as creating new phases of matter and loss of tunneling

which are corroborated using Floquet theory coupled to adiabatic master equations²¹⁻²⁵. Further, adiabatic master equations developed by modulating two system parameters have been shown to break nonequilibrium fluctuation theorems and TUR because of the emergence of geometric phaselike quantities^{17,26-29}. Although driven QHEs (dQHEs) have not yet been experimentally realized, driven molecular junctions (theory of which is akin to QHEs) have been experimentally studied where geometric phaselike effects were proven to exhibit non-standard influence on transport properties as predicted by adiabatic master equations^{30,31}. With the current experimental realization of QHEs and driven molecular junctions, it is not far that, driven dynamics predicted by adiabatic master equations can be soon compared with experimental results.

There are several ways of driving the internal parameters of a dQHE. A particular example includes a stepwise sweep of the temperatures of the thermal reservoirs³². Such periodic driving protocols have led to the development of a quantum version of TUR signifying a trade-off between entropy production rate and signal to noise ratio³². Interestingly, over the past couple of years, several TUR have been developed in quantum engines³³⁻³⁶. In a previous study we have showed that, such a trade-off is invalid in presence of continuous driving of the temperatures of the two baths in a sinusoidal manner²⁷. We have also showed how other thermodynamic quantities of a popular QHE model such as flux, noise, efficiency, power etc. are influenced by such drivings^{27,37}. Notably, we showed the universal linear slope of 1/2 in the standard efficiency at maximum power (EMP) as a function of Carnot

^{a)}Electronic mail: hpg@gauhati.ac.in

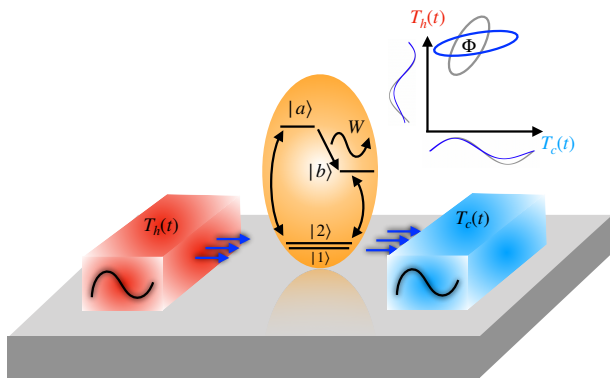


FIG. 1. Schematic plot of an amplitude modulated driven 4 level QHE. Two degenerate states $|1\rangle$ and $|2\rangle$ are coupled with higher energy states $|a\rangle$ and $|b\rangle$ through respective thermal baths. The state $|a\rangle$ is higher in energy than the state $|b\rangle$. Hot and cold bath temperatures are labeled as $T_h(t)$ and $T_c(t)$ respectively. States $|a\rangle$ and $|b\rangle$ are also coupled with a unimodal cavity. During the transition from $|a\rangle$ to $|b\rangle$ one photon is produced in the cavity with an energy equal to the energy difference between these states which we treat as work done by the system denoted by W . Temperature amplitude shaping modifies the induced geometric phase Φ shown in the upper inset.

efficiency (η_c) no longer holds when there is a finite phase difference between the two continuous driving protocols²⁷. A natural question is how would the thermodynamic quantities behave when the continuous driving is replaced by an amplitude modulated driving (similar to a single cycle pulse). To keep things simple, we first focus on the adiabatic limit, where there are no sudden modulation or pulse induced dynamics in the engine, i.e, the driving timescale is well separated from the engine-evolution timescale. By considering two type of envelope functions Gaussian and Lorentzian, we note some interesting observations and compare the results obtained with the known continuous sinusoidal driving which is the limiting case with large envelope width.

This paper is organized as follows. In Sec.II, we briefly introduce the model and discuss the basic underlying principles. In Sec.III, we present our results and offer a discussion followed by the concluding remarks in Sec.IV.

II. AMPLITUDE MODULATED DRIVEN QUANTUM HEAT ENGINE

We consider a four level temperature driven quantum heat engine coupled with two thermal baths and a unimodal cavity, Fig.(1). This model has been studied in several previous works^{27,38-41}. The theoretical

framework has already been developed and discussed before^{27,37} and we refer to the appendix for necessary details. The engine operates in such a way that two thermal baths at temperatures $T_h(t)$ and $T_c(t)$, are adiabatically driven externally. The driving protocol is cyclic whose amplitude is being modulated in time thus shaping the envelope, which we refer to as *amplitude modulation*. We choose the following driving protocols,

$$T_c(t) = T_{c0} + A_i(t) \sin(\omega t), \quad (1)$$

$$T_h(t) = T_{h0} + A_i(t) \sin(\omega t + \phi), \quad (2)$$

where A_i is expressed as

$$A_S(t) = A_0, \quad (3)$$

$$A_G(t) = A_0 \exp\left(-4 \ln 2 \frac{t^2}{t_e^2}\right), \quad (4)$$

$$A_L(t) = A_0 \frac{[t_e/2]^2}{t^2 + [t_e/2]^2}, \quad (5)$$

with $i \in (S, G, L)$. Here t_e is termed as envelope duration and $A_i(t)$ is the envelope type such that the subscript i represents the type of envelope – constant, Gaussian, or Lorentzian. Note that t_e is the full-width at half maximum (FWHM) for both Gaussian and Lorentzian envelopes. A_0 , ω and ϕ are amplitude, frequency and phase difference between the driving protocols respectively. Here the cold (hot) bath temperature oscillates around $T_{c0}(T_{h0})$. Bath temperatures are periodically driven in time such that $T_h(t) > T_c(t)$ condition is maintained throughout. Note that, the geometric contributions get explicitly added to the engine's thermodynamic properties due to the periodic driving of the reservoir temperatures. It is finite only when the driving protocols are phase different (which is introduced as a phase difference ϕ)³⁷. Although we can observe driven dynamics when $\phi = 0$, geometric contributions change the driven dynamics if and only if $\phi \neq 0$. In this QHE, the exact analytical nature of the relationship between geometric effects and ϕ is however not known and so we resort to numerics to gain insights on its role on the thermodynamics. Throughout the text, whenever we refer to the phrase '*in the presence of geometric contributions*', we mean $\phi \neq 0$ in the driving protocols. The central quantity of interest in this work is the effect of geometric contributions on the thermodynamics of the QHE. The work done by the engine W is quantified as energy flow (in the form of photon) into the cavity during the transition from $|a\rangle$ to $|b\rangle$. The hot and cold reservoirs induce coherence in the reduced system density matrix and they are denoted as p_h and p_c respectively⁴². Through the amplitude modulation in the driving protocols, the additional parameter FWHM (or envelope duration), t_e , allows us to control the overall geometric contributions to the thermodynamics of the QHE. In the next sections, we focus on the thermodynamic quantities as a function of the control parameters, viz. envelope duration, t_e and

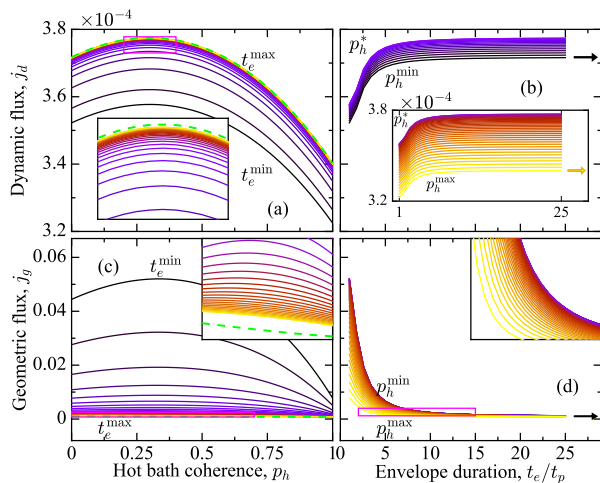


FIG. 2. Graphical representation of the dynamic (panel (a) and (b)) and geometric (panel (c) and (d)) fluxes as a function of p_h (left) for different t_e values ($t_e^{\min} = t_p$, $t_e^{\max} = 25t_p$) and as a function of t_e (right) for different p_h values ($p_h^{\min} = 0$, $p_h^{\max} = 1$) for a Gaussian envelope $A_G(t)$. (a) Dynamic flux j_d is optimized with p_h at various t_e . t_e increases from bottom to top. (b) j_d as a function of a dimensionless envelope duration, t_e/t_p (see text for interpretation). (c) Optimization of geometric flux j_g at finite envelope widths. t_e decreases from bottom to top. Inset shows dashed line where optimization is not possible for the sinusoidal driving. (d) Decrease in j_g with t_e . Arrows in (b) and (d) indicate fluxes for a sinusoidal driving for maximum (yellow) and minimum (black) p_h values and p_h^* is the optimized p_h for dynamic flux. Here: $T_{c0} = 1.0$, $T_{h0} = 1.67$, $t_l = 2$, $E_1 = E_2 = 0.1$, $E_b = 0.4$, $E_a = 1.5$, $A_0 = 0.01$, $\omega = 2500$, $p_c = 0.3$, $r = 0.1$, $g = 40$, $\tau = 0.01$, $\phi = \pi/2$. Atomic units are considered throughout.

the hot bath induced coherence parameter, p_h .

III. RESULTS AND DISCUSSION

A. Flux and Noise

The net photon flux exchanged between the engine and cavity is a fluctuating quantity. Both the flux (j) and the noise or fluctuations (n) in photon exchange are measurable quantities and are composed of additive dynamic (subscript d) and geometric parts (subscript g) given by³⁷,

$$j = j_d + j_g, \quad (6)$$

$$n = n_d + n_g. \quad (7)$$

The quantities, $j_d(j_g)$ are the first order dynamic (geometric) cumulants and $n_d(n_g)$ are the second order dynamic (geometric) cumulants which can be obtained directly from a cumulant generating function described in the appendix (Eq.16 and Eq.17). Fig.2 and Fig.3 display the behavior of the flux and the noise respectively

for the Gaussian envelope $A_G(t)$ (Eq.4) as a function of the hot bath induced coherence p_h and envelope duration t_e in the unit of driving period t_p . It is interesting to notice the two extremum limit of the envelope $A_G(t)$: (i) It becomes a Dirac-delta function $A_0\delta(t)$ when $t_e \rightarrow 0$ and (ii) In the opposite limit, $t_e \rightarrow \infty$, it becomes $A_S(t)$ (Eq.3) i.e., a sinusoidal driving.

In Fig.(2a), j_d is plotted as a function of p_h for increasing t_e (bottom to top) and in Fig.(2b) j_d is plotted against t_e for the range $0 \leq p_h \leq 1$. For all t_e values, j_d is optimizable with p_h and the optimized p_h (p_h^*) is independent of t_e . j_d increases with t_e rapidly and then saturates to the sinusoidal driving (green dashed line in Fig.(2a) and arrows for two different p_h values in Fig.(2b)). In Fig.(2b), one clearly sees that the saturation threshold (the minimum value of t_e for the saturation) does not depend on p_h .

In Fig.(2c) and Fig.(2d), the geometric flux j_g is evaluated for the full range of p_h and t_e . As a function of p_h , j_g shows a remarkably different behavior than j_d , where we see optimization of the flux when t_e is smaller than a critical value. This is in contrast to what we observed earlier for sinusoidal driving, where we reported that optimization was not possible in case of j_g as a function of p_h ²⁷. But upon envelope modulation, the optimization is possible below a critical t_e value. Contrary to the dynamic flux optimization, the optimal value of hot bath induced coherence, p_h^* , at which we see the optimized geometric flux, is dependent on t_e . Further, j_g decreases as t_e increases and eventually approaches sinusoidal driving (green dashed line in Fig.(2c) and arrows for the two different p_h values in Fig.(2d)) which is complementary to the behavior of j_d .

The dynamic (n_d) and geometric (n_g) noise are displayed in Fig.(3) spanning the full range of p_h and t_p . In Fig.(3a), we have showed that n_d is optimizable as a function of p_h for all values of t_e . Interestingly, we observe that the optimization of flux and noise occurs at the same value of p_h^* , $p_h^* = 0.3$ for the considered parameters. Further, the noise does not change with t_e and remains constant as the sinusoidal driving (green dashed line in Fig.(3a) and arrows in Fig.(3b)). This behavior is also reflected in Fig.(3b), where n_d for all values of p_h is shown to be independent of t_e . In Fig.(3c), the geometric noise is calculated with respect to p_h (t_e increases from bottom to top). As t_e is decreased, n_g starts exhibiting optimizable character. This behavior is similar to that of j_g . The difference is that, where j_g decreases, n_d increases with t_e , as shown in Fig.(3d). In Fig.(3d), we see that n_g sharply increases at lower values of t_e and saturates to the value obtained from sinusoidal driving (green dashed line in Fig.(3c) and arrows in Fig.(3d)) at different evaluated values of p_h .

In Fig.(4), we show the dependence of the envelope

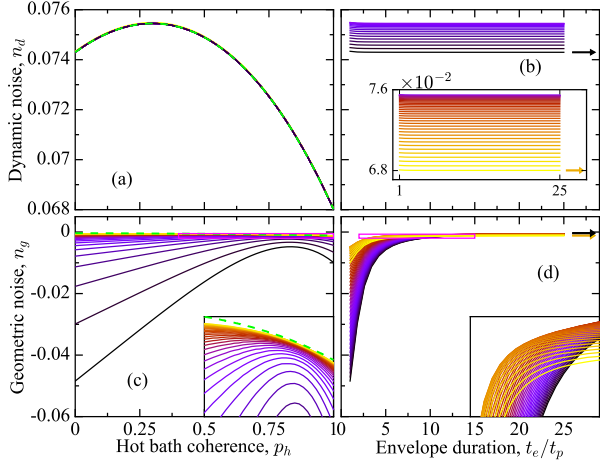


FIG. 3. Dynamic ((a), and (b)) and geometric ((c), and (d)) noise for the driving with Gaussian envelope $A_G(t)$. Same color code is used as in Fig.2. Green dashed lines are for $A_S(t)$ envelope. (a) Optimization of the dynamic noise n_d as a function of hot bath coherence p_h for different values of t_e . Note that, the envelope shape and duration has no effect on the optimization of the dynamic noise. (b) n_d as a function of envelope duration t_e for different values of p_h . From blue to yellow p_h increases from $p_h = p_h^*$ to $p_h = 1$ and in the inset from black to blue p_h increases from $p_h = 0$ to $p_h = p_h^*$. (c) Optimization of the geometric noise n_g as a function of p_h for different values of t_e . (d) Behavior of n_g with t_e for different values of p_h . In (b) and (d), black and yellow arrows represent the noise for $A_S(t)$ envelope for $p_h = 0$ and $p_h = 1$ respectively.

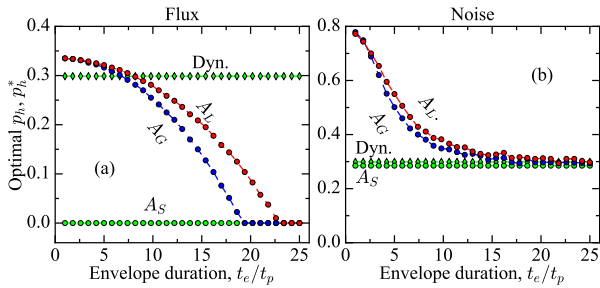


FIG. 4. Variation of the optimal value of hot bath coherence p_h^* , as a function of envelope duration t_e in the unit of t_p for (a) flux and (b) noise. Total (dynamic + geometric) contributions are plotted along with the dynamic contribution (green diamond points) for three different envelopes – sinusoidal (green circles, Eq.3), Gaussian (blue circles, Eq.4), and Lorentzian (red circles, Eq.5)). Dynamic contribution does not depend on the envelope shape.

duration t_e on the optimal coherence p_h^* for the dynamic and total (dynamic + geometric) flux (j) as well as noise (n). In Fig.(4a), the line at $p_h^* = 0.3$ (green diamonds) represents the j_d value and highlights the independence of p_h^* on the envelope shape and duration t_e . The line at $p_h^* = 0$ (green circles) represents the total flux when there is a sinusoidal driving. In the latter case, the to-

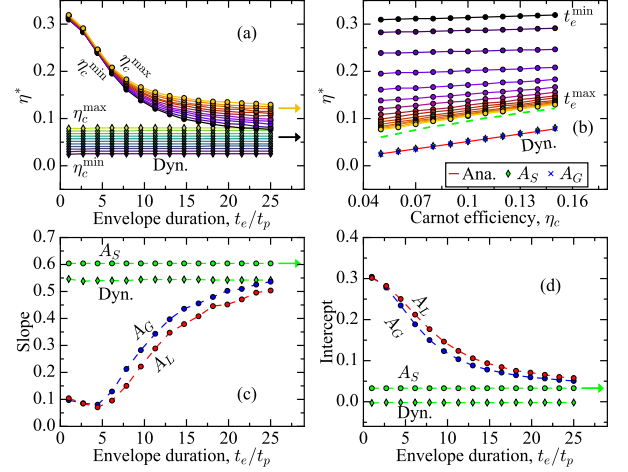


FIG. 5. (a) Efficiency at maximum power η^* for dynamic (blue to yellow lines) and total (black to orange lines) contributions as a function of envelope duration t_e for increasing Carnot efficiency η_c from bottom to top ($\eta_c^{\min} = 0.04$ and $\eta_c^{\max} = 0.15$). Black and yellow arrows represent the values of η^* for $A_S(t)$ envelope (Eq.3) for minimum and maximum values of considered η_c respectively. (b) η^* as function of η_c for different values of t_e (black to yellow lines t_e increases). Green dashed line is for $A_S(t)$ envelope (Eq.3). Red line is obeying the standard equation $\eta^* = \eta_c/2$, Eq.11. Green diamond and blue cross points represent dynamic part of $A_S(t)$ (Eq.3) and $A_G(t)$ (Eq.4) envelopes respectively. (c) Slopes for the lines in panel (b). Green diamond points represent the dynamic contribution (does not depend on the envelope shape). Green, blue, and red circles are for total (dynamic + geometric) contributions for $A_S(t)$ (Eq.3), $A_G(t)$ (Eq.4), and $A_L(t)$ (Eq.5) envelopes respectively. (d) Same as panel (c) but intercepts for the lines in panel (b).

tal flux is dominated by the geometric contribution and the optimized values of flux occur at $p_h = 0$, as known previously²⁷. In presence of modulated drivings (both Gaussian and Lorentzian), unlike the sinusoidal driving, the value of p_h^* smoothly decreases from a large value as we keep increasing t_e depending on the shape of the envelope. In Fig.(4b), for the dynamic noise (green diamonds) the optimal value of p_h^* is independent of envelope shape and duration and also p_h^* does not depend on t_e for the sinusoidal driving (similar to what was observed for the flux). p_h^* value is however larger in presence of amplitude modulation (Lorentzian or Gaussian) and gradually meets the sinusoidal driving as t_e increases again depending on the shape of the envelope.

B. Efficiency and Uncertainty Relationship

The work done by the engine is the stimulated emission of photons into a unimodal cavity coupled to the higher

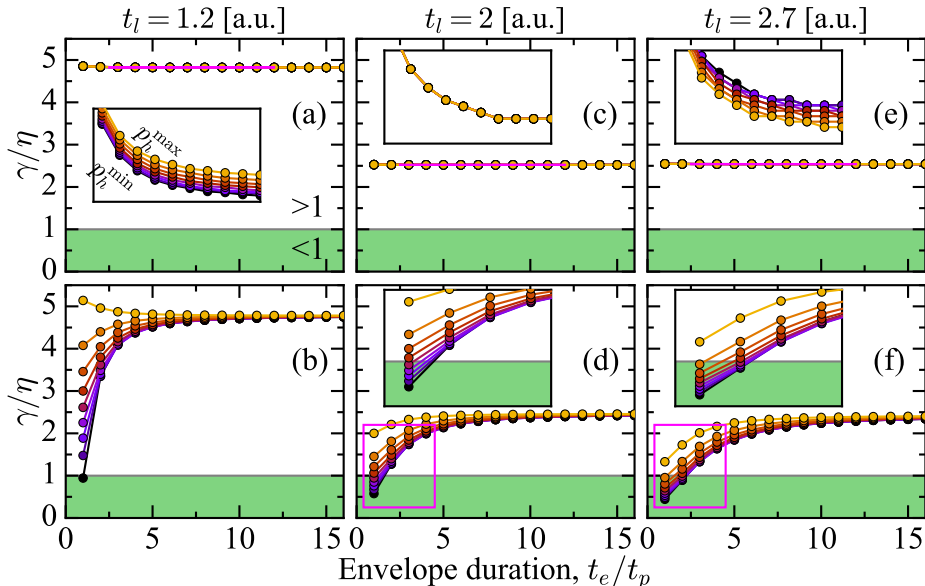


FIG. 6. γ/η for dynamic (top) and total (bottom) contributions as a function of envelope duration t_e for (a, b) $t_l = 1.2$, (c, d) $t_l = 2$, and (e, f) $t_l = 2.7$, in the range $0 \leq p_h \leq 1$.

energy states of the engine which is given by³⁹,

$$W = E_a - E_b + \frac{1}{t_p} \ln \frac{(1 + n_l)}{n_l} \int_0^{t_p} dt' T_c(t'). \quad (8)$$

n_l is the cavity Bose-Einstein occupation factor expressed as $n_l = 1/(\exp[(E_a - E_b)/t_l] - 1)$ with t_l being the temperature of the cavity³⁹. The power can be expressed as,

$$P = W(j_d + j_g) = Wj. \quad (9)$$

The efficiency of the system can be written as $\eta = W/(E_a - E_1)$ and the efficiency at maximum power, η^* , can be obtained by optimizing η with respect to an engine parameter (here we choose E_b). A popular analytical expression for η^* , called the Curzon-Ahlborn efficiency at maximum power, can be written in terms of the Carnot efficiency, η_c , given by

$$\eta^* = 1 - \sqrt{1 - \eta_c} \quad (10)$$

$$= \frac{\eta_c}{2}, \text{ near equilibrium.} \quad (11)$$

The linear coefficient, $1/2$ has been claimed to be universal^{43,44}, which we showed was violated in presence of geometric effects²⁷ with sinusoidal drivings. Here, we evaluate η^* as a function of the envelope duration t_e of the modulated driving and compare the results with Eq.(11). In Fig.(5a), we show the behavior of η^* with respect to t_e for the range $0.05 < \eta_c < 0.15$ (bottom to top). The total η^* is maximum (> 0.3) when the envelope duration is minimum ($t_e = t_p$). η^* non-linearly decreases as t_e increases and eventually saturates to the value obtained from sinusoidal drivings at large t_e .

The lower set of curves (parallel lines) correspond to η^* values, when there are no geometric contributions (only dynamic). Here, η^* does not depend on t_e . In Fig.(5b), we show that η^* linearly increases with η_c , but the slope is $1/2$ only when geometric contributions are absent (holds for dynamic, green diamond and blue cross points). Further, t_e has no effect on the slope under the same conditions. However, in presence of geometric effects, this slope of $1/2$ is not maintained anymore. The behavior of the slope and intercept in presence of geometric effects is shown graphically in Figs.(5 c and d) respectively. The slope decreases, reaches a minimum, and then gradually increases and saturates at the respective values obtained for sinusoidal case, for both Gaussian and Lorentzian drivings. Note that, as per Eq.(11), there is no intercept in η^* as a function of η_c . In presence of geometric effects, an intercept is introduced in the standard expression because of the driven dynamics. This intercept non-linearly decreases with t_e and approaches the value obtained from sinusoidal drivings.

Efficiency, being one of the most characteristic quantity of engines is often deeply investigated to gain deeper thermodynamic insights. During the last two years, with respect to QHE, several interesting bounds on efficiency have been proposed⁴⁵, especially derived from TUR³³. One of such bounds on the efficiency of QHEs is given by³²,

$$\gamma/\eta \geq 1, \text{ with } \gamma = \frac{\eta_c P}{T_c \dot{\Sigma} + P}, \quad (12)$$

where $\dot{\Sigma}$ represents the rate of entropy production and

has been claimed to be a direct result of TUR in quantum systems³⁵. The average entropy production is given by $\Sigma = j\mathcal{A}$, where \mathcal{A} is the thermodynamic affinity⁴⁶. Using an established TUR of the type $\mathcal{A}n/j \geq 2k_B$ ⁴⁶, it is straight-forward to recast Eq.(12) to $(k_B \rightarrow 1)$,

$$\gamma/\eta \geq 1, \quad \text{with } \gamma = \frac{\eta_c P}{P + T_c \mathcal{A} j}. \quad (13)$$

It is natural to see the validity of the Eq.(13) in presence of geometric effects as well as other engine parameters. In our engine, the thermodynamic affinity is known and is given by³⁷ $\mathcal{A} = \ln \frac{\tilde{n}_l \int_0^{t_p} dt' [1+n_c(t')]n_h(t')}{n_l \int_0^{t_p} dt' n_c(t')[1+n_h(t')]}$. We numerically evaluate γ and η in Eq.(13) and plot γ/η as a function of envelope duration, t_e in Fig.(6), evaluated at different cavity temperatures t_l and coherence values p_h . In the panels (a), (c), and (e), there are no geometric contributions (only dynamic, $\phi = 0$) and the inequality $\gamma/\eta > 1$ is always maintained irrespective of any engine parameters. From the insets, we show that γ/η changes its order with respect to p_h as t_l increases (panel (a) to (e)). Most interestingly, in the presence of geometric contribution (panel (b), (d), and (f)), by suitably selecting t_l and t_e we report a region where the inequality Eq.13 does not hold. This happens at very small values of t_e and large values of t_l where we observe that $\gamma/\eta < 1$. As t_e increases and the driving approaches the value obtained from sinusoidal drivings where the inequality is recovered. Therefore, the inequality condition is broken only in the presence geometric effects introduced due to amplitude modulation. If the amplitude modulation is absent, the inequality holds.

IV. CONCLUSION

In this work, we chose to drive the two temperatures of the thermal reservoirs of a quantum heat engine with protocols where the driving amplitude is being modulated in the adiabatic limit introducing envelope functions. With such amplitude modulation, we reported the optimization of the geometric flux with respect to quantum coherences for a finite envelope duration, which is otherwise not possible with simple sinusoidal drivings. Further, we also optimized the dynamic as well as the geometric noise and this optimization is independent of envelope duration for the former one whereas for the later one optimization point is envelope duration dependent. The optimal value of coherence decreases as the envelope duration is increased depending on the shape of envelope. Another interesting thermodynamics quantity, the efficiency at maximum power (EMP), decreases non-linearly with the envelope duration. In the presence of both geometric effects and modulated driving with envelope, the slope and intercept arises, which deviate from the standard linear expression for EMP in terms of Carnot efficiency in an

intricate manner depending on the shape and duration of the envelope. Further, universal bounds on efficiency based on uncertainty relationships does not hold when geometric effects are employed via amplitude modulation with shorter envelope duration and larger cavity temperatures.

APPENDIX

The QHE has degenerate quantum states $|1\rangle$ and $|2\rangle$, with same symmetry (therefore with a forbidden transition between them) are coupled to two thermal baths. The higher energy states $|a\rangle$ and $|b\rangle$ with different symmetry and allowed transition between them are coupled to the hot and cold bath respectively. The state $|a\rangle$ is higher in energy than the state $|b\rangle$. $|1\rangle$, $|2\rangle$, $|b\rangle$ and $|a\rangle$ states correspond to the energies of E_1 , E_2 , E_b and E_a respectively. States $|a\rangle$ and $|b\rangle$ are also coupled to a unimodal cavity and the strength of the coupling is denoted by g . With above assumptions the total Hamiltonian can be written as $\hat{H}_T = \hat{H}_0 + \hat{V}_{sb} + \hat{V}_{sc}$, where

$$\begin{aligned} \hat{H}_0 &= \sum_{\nu=1,2,a,b} E_\nu |\nu\rangle\langle\nu| + \sum_{k \in h,c} \epsilon_k \hat{a}_k^\dagger \hat{a}_k + \epsilon_l \hat{a}_l^\dagger \hat{a}_l, \\ \hat{V}_{sb} &= \sum_{k \in h,c} \sum_{i=1,2} \sum_{x=a,b} r_{ik} \hat{a}_k |x\rangle\langle i| + \text{H.c.}, \\ \hat{V}_{sc} &= g \hat{a}_l^\dagger |b\rangle\langle a| + \text{H.c.} \end{aligned} \quad (14)$$

In the above equation, E_ν , ϵ_k and ϵ_l are the energy of the system's ν th level, k th mode of the thermal reservoirs and unimodal cavity respectively. r_{ik} is the system-reservoir coupling of the i th state with the k th mode of the reservoirs. Thermal baths are modeled as harmonic modes with \hat{a}^\dagger (\hat{a}) being the bosonic creation (annihilation) operators. There is a heat flow from the hot bath to the cold bath in a nonlinear fashion. Also, there is a radiative decay channel originates from the transition $|a\rangle \rightarrow |b\rangle$.

Apropos to the theoretical formalism in the Liouville space, presented in our earlier works^{27,37}, a reduced density vector in the Liouville space is composed of the four coupled population and a coherence given by $|\rho(\lambda, t)\rangle = \{\rho_{11}, \rho_{22}, \rho_{aa}, \rho_{bb}, \Re(\rho_{12})\}$, with $i = 1, 2, a, b$ which denotes the system's many body states and $\Re(\rho_{12})$ is the thermally induced coherence between states $|1\rangle$ and $|2\rangle$. An adiabatic Markovian quantum master equation approach combined with a standard generating function technique allows us to evaluate the statistics of photons exchanged between the engine and cavity as per the equation $\dot{\rho}(\lambda, t) = \check{\mathcal{L}}(\lambda, t)|\rho(\lambda, t)\rangle$, where λ is a field that counts the number of photons exchanged between the system and the cavity. $\check{\mathcal{L}}(\lambda, t)$ is the adiabatic effective evolution Liouvillian superoperator within the Markov approximation, given by

$$\check{\mathcal{L}}(\lambda, t) = \begin{pmatrix} n_1(t) & 0 & r_{1h}\tilde{n}_h(t) & r_{1c}\tilde{n}_c(t) & y(t) \\ 0 & n_2(t) & r_{2h}\tilde{n}_h(t) & r_{2c}\tilde{n}_c(t) & y(t) \\ r_{1h}n_h(t) & r_{2h}n_h(t) & -g^2\tilde{n}_l - 2r_h\tilde{n}_h(t) & g^2n_l e^{-\lambda} & 2r_h p_h n_h(t) \\ r_{1c}n_c(t) & r_{2c}n_c(t) & g^2\tilde{n}_l e^{\lambda} & -g^2n_l - 2r_c\tilde{n}_c(t) & 2r_c p_c n_c(t) \\ \frac{y(t)}{2} & \frac{y(t)}{2} & r_h p_h \tilde{n}_h(t) & r_c p_c \tilde{n}_c(t) & -n(t) \end{pmatrix} \quad (15)$$

In the above equation $n_i(t) = -[r_{ic}n_c(t) + r_{ih}n_h(t)]$ with $i = 1, 2$, $r_c = r_{1c} + r_{2c}$, $r_h = r_{1h} + r_{2h}$, $y(t) = -r_c n_c(t) p_c - r_h n_h(t) p_h$, $\tilde{n}_c(t) = n_c(t) + 1$, $n(t) = (r_{1h} + r_{2h})n_h(t)/2 + (r_{1c} + r_{2c})n_c(t)/2 + \tau$, $\tilde{n}_h(t) = n_h(t) + 1$, $\tilde{n}_l = 1 + n_l$ and τ is an environmental dephasing parameter. In this study we have considered equal system-reservoir coupling denoted by r . The explicit form of $n_c(t)$ and $n_h(t)$ can be expressed as $n_c(t) = 1/(\exp\{(E_b - E_1)/k_B T_c(t)\} - 1)$, $n_h(t) = 1/(\exp\{(E_a - E_1)/k_B T_h(t)\} - 1)$. p_h and p_c is the quantum coherence control parameters associated with the hot and cold baths respectively.

The statistics of q (number of photons exchanged between the system and the cavity) is obtained from moment generating function, which is expressed as $G(\lambda, t) = \sum_q e^{\lambda q} P(q, t)$ where $P(q, t)$ is the probability distribution function corresponding to q net photons in the cavity within a measurement window, t . Within the full counting statistics (FCS) formalism, it can be shown that $\dot{G}(\lambda, t) = \langle \check{\mathbf{1}} | \check{\mathcal{L}}(\lambda, t) | \rho(\lambda, t) \rangle$ with $\langle \check{\mathbf{1}} | = \{1, 1, 1, 1, 0\}$ ^{47,48}. With the help of Eq.(15), one can obtain geometric contributions from the scaled cumulant generating function given by $S(\lambda) = \lim_{t \rightarrow \infty} (1/t) \ln[\langle \check{\mathbf{1}} | \exp(\check{\mathcal{L}}(\lambda, t)t) | \rho(\lambda, t) \rangle]$. $S(\lambda)$ is separable into dynamic and geometric parts additively, $S(\lambda, t) = S_d(\lambda, t) + S_g(\lambda, t)$,

$$S_d(\lambda) = \frac{1}{t_p} \int_0^{t_p} dt' \zeta_o(\lambda, t'), \quad (16)$$

$$S_g(\lambda) = -\frac{1}{t_p} \int_0^{t_p} \langle L_o(\lambda, t) | \dot{R}_o(\lambda, t) \rangle dt. \quad (17)$$

In the above equation, $S_d(\lambda)$ and $S_g(\lambda)$ represent the dynamic and geometric cumulant generating function respectively. $|R_o(\lambda, t)\rangle$ and $\langle L_o(\lambda, t)|$ are the instantaneous right and left eigenvectors of $\check{\mathcal{L}}(\lambda, t)$ with instantaneous long-time dominating eigenvalue, $\zeta_o(\lambda, t)$. Note that, analytical expressions for both $S_d(\lambda)$ and $S_g(\lambda)$ cannot be derived for 4 level dQHE. The cumulant generating function are analytically known only for two level systems^{29,31} within the Markov limits. Systems with large number of states, analytical expressions have not been reported since the geometric contributions involve calculation of both the left and right eigenvectors of the Hamiltonian. The n th order fluctuations (cumulants of $S(\lambda)$) can be calculated as

$$C_d^{(i)} = \partial_\lambda^i S_d(\lambda)|_{\lambda=0}, \quad (18)$$

$$C_g^{(i)} = \partial_\lambda^i S_g(\lambda)|_{\lambda=0}. \quad (19)$$

When $i = 1$, we get the dynamic (geometric) flux, $j_d(j_g)$, and when $i = 2$, we obtain the dynamic (geometric) noise, $n_d(n_g)$, which are numerically evaluated.

ACKNOWLEDGMENTS

HPG acknowledges the support from Science and Engineering Board for the start-up grant, SERB/SRG/2021/001088.

- ¹H. Scovil and E. Schulz-DuBois, "Three-level masers as heat engines," Phys. Rev. Lett. **2**, 262 (1959).
- ²Y. Zou, Y. Jiang, Y. Mei, X. Guo, and S. Du, "Quantum heat engine using electromagnetically induced transparency," Phys. Rev. Lett. **119**, 050602 (2017).
- ³J.-P. Brantut, C. Grenier, J. Meineke, D. Stadler, S. Krinner, C. Kollath, T. Esslinger, and A. Georges, "A thermoelectric heat engine with ultracold atoms," Science **342**, 713–715 (2013).
- ⁴J. Klatzow, J. N. Becker, P. M. Ledingham, C. Weinzetl, K. T. Kaczmarek, D. J. Saunders, J. Nunn, I. A. Walmsley, R. Uzdin, and E. Poem, "Experimental demonstration of quantum effects in the operation of microscopic heat engines," Phys. Rev. Lett. **122**, 110601 (2019).
- ⁵G. Maslennikov, S. Ding, R. Hablützel, J. Gan, A. Roulet, S. Nimmrichter, J. Dai, V. Scarani, and D. Matsukevich, "Quantum absorption refrigerator with trapped ions," Nature communications **10**, 1–8 (2019).
- ⁶J. Roßnagel, S. T. Dawkins, K. N. Tolazzi, O. Abah, E. Lutz, F. Schmidt-Kaler, and K. Singer, "A single-atom heat engine," Science **352**, 325–329 (2016).
- ⁷J. P. Peterson, T. B. Batalhao, M. Herrera, A. M. Souza, R. S. Sarthour, I. S. Oliveira, and R. M. Serra, "Experimental characterization of a spin quantum heat engine," Phys. Rev. Lett. **123**, 240601 (2019).
- ⁸N. M. Myers, O. Abah, and S. Deffner, "Quantum thermodynamic devices: from theoretical proposals to experimental reality," arXiv preprint arXiv:2201.01740 (2022).
- ⁹G. Benenti, G. Casati, K. Saito, and R. S. Whitney, "Fundamental aspects of steady-state conversion of heat to work at the nanoscale," Physics Reports **694**, 1–124 (2017).
- ¹⁰S. Pal, T. Mahesh, and B. K. Agarwalla, "Experimental demonstration of the validity of the quantum heat-exchange fluctuation relation in an nmr setup," Physical Review A **100**, 042119 (2019).
- ¹¹D. Mayer, F. Schmidt, S. Haupt, Q. Bouton, D. Adam, T. Lausch, E. Lutz, and A. Widera, "Nonequilibrium thermodynamics and optimal cooling of a dilute atomic gas," Physical Review Research **2**, 023245 (2020).
- ¹²S. Hernández-Gómez, N. Staudenmaier, M. Campisi, and N. Fabbri, "Experimental test of fluctuation relations for driven open quantum systems with an nv center," New Journal of Physics **23**, 065004 (2021).
- ¹³K. Li, Y. Xiao, J. He, and J. Wang, "Performance of quantum heat engines via adiabatic deformation of potential," arXiv preprint arXiv:2202.06651 (2022).
- ¹⁴K. Brandner, M. Bauer, and U. Seifert, "Universal coherence-induced power losses of quantum heat engines in linear response," Phys. Rev. Lett. **119**, 170602 (2017).

- ¹⁵J. Liu, K. A. Jung, and D. Segal, “Periodically driven quantum thermal machines from warming up to limit cycle,” *Phys. Rev. Lett.* **127**, 200602 (2021).
- ¹⁶B. Cakmak and Ö. E. Müstecaplıoğlu, “Spin quantum heat engines with shortcuts to adiabaticity,” *Phys. Rev. E* **99**, 032108 (2019).
- ¹⁷K. Takahashi, Y. Hino, K. Fujii, and H. Hayakawa, “Full counting statistics and fluctuation–dissipation relation for periodically driven two-state systems,” *Journal of Statistical Physics* **181**, 2206–2224 (2020).
- ¹⁸W. Niedenzu and G. Kurizki, “Cooperative many-body enhancement of quantum thermal machine power,” *New Journal of Physics* **20**, 113038 (2018).
- ¹⁹B. Bhandari, P. T. Alonso, F. Taddei, F. von Oppen, R. Fazio, and L. Arrachea, “Geometric properties of adiabatic quantum thermal machines,” *Phys. Rev. B* **102**, 155407 (2020).
- ²⁰J. Eglinton and K. Brandner, “Geometric bounds on the power of adiabatic thermal machines,” arXiv preprint arXiv:2202.08759 (2022).
- ²¹S. Scopa, G. T. Landi, and D. Karevski, “Lindblad-floquet description of finite-time quantum heat engines,” *Physical Review A* **97**, 062121 (2018).
- ²²T. Albash, S. Boixo, D. A. Lidar, and P. Zanardi, “Quantum adiabatic markovian master equations,” *New J. Phys.* **14**, 123016 (2012).
- ²³B. Ye, F. Machado, and N. Y. Yao, “Floquet phases of matter via classical prethermalization,” *Physical Review Letters* **127**, 140603 (2021).
- ²⁴S. Restrepo, J. Cerrillo, P. Strasberg, and G. Schaller, “From quantum heat engines to laser cooling: Floquet theory beyond the born–markov approximation,” *New Journal of Physics* **20**, 053063 (2018).
- ²⁵R. Dann, A. Levy, and R. Kosloff, “Time-dependent markovian quantum master equation,” *Physical Review A* **98**, 052129 (2018).
- ²⁶Z. Wang, L. Wang, J. Chen, C. Wang, and J. Ren, “Geometric heat pump: Controlling thermal transport with time-dependent modulations,” *Frontiers of Physics* **17**, 1–14 (2022).
- ²⁷S. K. Giri and H. P. Goswami, “Geometric phaselike effects in a quantum heat engine,” *Phys. Rev. E* **96**, 052129 (2017).
- ²⁸T. Simons, D. Meidan, and A. Romito, “Pumped heat and charge statistics from majorana braiding,” *Physical Review B* **102**, 245420 (2020).
- ²⁹J. Ren, P. Hänggi, and B. Li, “Berry-phase-induced heat pumping and its impact on the fluctuation theorem,” *Phys. Rev. Lett.* **104**, 170601 (2010).
- ³⁰J. Gu, X.-G. Li, H.-P. Cheng, and X.-G. Zhang, “Adiabatic spin pump through a molecular antiferromagnet Ce3Mn8III ,” *The Journal of Physical Chemistry C* **122**, 1422–1429 (2018).
- ³¹H. P. Goswami, B. K. Agarwalla, and U. Harbola, “Geometric effects in nonequilibrium electron transfer statistics in adiabatically driven quantum junctions,” *Phys. Rev. B* **93**, 195441 (2016).
- ³²H. J. Miller, M. H. Mohammady, M. Perarnau-Llobet, and G. Guarnieri, “Thermodynamic uncertainty relation in slowly driven quantum heat engines,” *Physical Review Letters* **126**, 210603 (2021).
- ³³J. M. Horowitz and T. R. Gingrich, “Thermodynamic uncertainty relations constrain non-equilibrium fluctuations,” *Nature Physics* **16**, 15–20 (2020).
- ³⁴P. Menczel, E. Loisa, K. Brandner, and C. Flindt, “Thermodynamic uncertainty relations for coherently driven open quantum systems,” *Journal of Physics A: Mathematical and Theoretical* **54**, 314002 (2021).
- ³⁵T. Koyuk and U. Seifert, “Thermodynamic uncertainty relation for time-dependent driving,” *Phys. Rev. Lett.* **125**, 260604 (2020).
- ³⁶Y. Hasegawa, “Thermodynamic uncertainty relation for general open quantum systems,” *Phys. Rev. Lett.* **126**, 010602 (2021).
- ³⁷S. K. Giri and H. P. Goswami, “Nonequilibrium fluctuations of a driven quantum heat engine via machine learning,” *Phys. Rev. E* **99**, 022104 (2019).
- ³⁸M. O. Scully, K. R. Chapin, K. E. Dorfman, M. B. Kim, and A. Svidzinsky, “Quantum heat engine power can be increased by noise-induced coherence,” *Proc. Natl. Acad. Sci. U.S.A.* **108**, 15097–15100 (2011).
- ³⁹H. P. Goswami and U. Harbola, “Thermodynamics of quantum heat engines,” *Phys. Rev. A* **88**, 013842 (2013).
- ⁴⁰S. Rahav, U. Harbola, and S. Mukamel, “Heat fluctuations and coherences in a quantum heat engine,” *Phys. Rev. A* **86**, 043843 (2012).
- ⁴¹U. Harbola, S. Rahav, and S. Mukamel, “Quantum heat engines: A thermodynamic analysis of power and efficiency,” *EPL (Europhysics Letters)* **99**, 50005 (2012).
- ⁴²A. A. Svidzinsky, K. E. Dorfman, and M. O. Scully, “Enhancing photocell power by noise-induced coherence,” *Coherent Optical Phenomena* **1**, 7–24 (2012).
- ⁴³C. Van den Broeck, “Thermodynamic efficiency at maximum power,” *Phys. Rev. Lett.* **95**, 190602 (2005).
- ⁴⁴M. Esposito, K. Lindenberg, and C. Van den Broeck, “Universality of efficiency at maximum power,” *Phys. Rev. Lett.* **102**, 130602 (2009).
- ⁴⁵J. M. Horowitz and T. R. Gingrich, “Thermodynamic uncertainty relations constrain non-equilibrium fluctuations,” *Nature Physics* **16**, 15–20 (2020).
- ⁴⁶B. K. Agarwalla and D. Segal, “Assessing the validity of the thermodynamic uncertainty relation in quantum systems,” *Phys. Rev. B* **98**, 155438 (2018).
- ⁴⁷L. S. Levitov and M. Reznikov, “Counting statistics of tunneling current,” *Phys. Rev. B* **70**, 115305 (2004).
- ⁴⁸M. Esposito, U. Harbola, and S. Mukamel, “Nonequilibrium fluctuations, fluctuation theorems, and counting statistics in quantum systems,” *Rev. Mod. Phys.* **81**, 1665–1702 (2009).